IOPscience

Magnetism and magnetoelectricity in the polar oxide -$Cu_2V_2O_7$

# Magnetism and magnetoelectricity in the polar oxide $\alpha$-Cu$_2$V$_2$O$_7$

Y.-W. Lee[1], T.-H. Jang[2,3], S. E. Dissanayake[4], Seunghun Lee[4] and Yoon H. Jeong[1(a)]

[1] *Department of Physics, Pohang University of Science and Technology - Pohang, 790-784, Korea*
[2] *c-CCMR, Pohang University of Science and Technology - Pohang, 790-784, Korea*
[3] *Max Planck POSTECH Center for Complex Phase Materials - Pohang, 790-784, Korea*
[4] *Department of Physics, University of Virginia - Charlottesville, VA 22904-4714, USA*

**Abstract** – Single crystals of the orthorhombic polar oxide $\alpha$-Cu$_2$V$_2$O$_7$ with space group $Fdd2$ are synthesized and their physical properties are measured. Neutron powder diffraction is also performed on a polycrystal sample to extract the magnetic structure. The ground state is shown to be weakly ferromagnetic, that is, collinearly antiferromagnetic in the $a$-direction with a small remanent magnetization in the $c$-direction. When an external magnetic field is applied in the $c$-direction, further spin canting, accompanied by the induced electric polarization, occurs. It is demonstrated that the magnetoelectric effect in $\alpha$-Cu$_2$V$_2$O$_7$ is adequately described if spin-dependent $p$-$d$ hybridization due to spin-orbit coupling as well as magnetic domain effects are simultaneously taken into account. We discuss the implication of the present result in the search for materials with multiferroicity and/or magnetoelectricity.

**Introduction.** – Over the past decade a considerable number of materials have been studied regarding multiferroics with simultaneous ferroelectricity and ferromagnetism in a single phase and/or magnetoelectricity arising from the cross coupling between them [1–3]. These materials belong to a rare system where both time reversal and space inversion symmetries are broken and the electric polarization can be manipulated by magnetic field and vice versa. From the latter aspect arises many technological application possibilities, and thus a proper understanding of the microscopic mechanisms is highly demanded.

On the theoretical front, there are presently at least three known microscopic mechanisms for magnetically induced ferroelectricity. Probably the most well-known mechanism is the spin current mechanism, or equivalently the inverse Dzyaloshinskii-Moriya (DM) mechanism [4,5]. In cycloidal spin structures, for example, the spin chirality can induce the polarization via the spin current mechanism. Orthorhombic perovskite TbMnO$_3$ is an example of the spin current mechanism [1]. It is also possible that even the collinear spin structure may induce ferroelectricity in crystals such as RMnO$_3$ (R = Ho, Tm, Yb) and TbMn$_2$O$_5$, if they contain inequivalent multiple magnetic sites [2]. In this case, polarization arises from magnetic striction caused by the symmetric exchange interaction [6]. This type of ferroelectricity would generally be realized in the so-called $E$-$type$ antiferromagnets ($\uparrow\uparrow\downarrow\downarrow$) [7]. Lastly a different kind, which is called the $p$-$d$ hybridization mechanism, was proposed to explain the ferroelectricity induced in the screw spin structures [8]. Here the ferroelectricity is supposedly caused by electronic charge transfer via the transition-metal-ligand $p$-$d$ hybridization which would depend on the spin direction due to spin-orbit coupling (SOC) [9]. Several materials such as melilite Ba$_2$CoGe$_2$O$_7$ [10,11] and borate (Cu,Ni)B$_2$O$_4$ [12] have been reported to follow this mechanism.

In this paper, we wish to report the successful growth of the single-crystalline $\alpha$-Cu$_2$V$_2$O$_7$ by the flux method and the measurements of the magnetic and electric properties of $\alpha$-Cu$_2$V$_2$O$_7$ samples in single crystalline as well as polycrystalline form. $\alpha$-Cu$_2$V$_2$O$_7$ is an oxide system of a peculiar structure with a potential for ferroelectricity, magnetoelectricity, and multiferroicity [13,14]. The physical properties and the field-induced polarization variations will be discussed based on the crystallographic, magnetic structure and magnetoelectric current measurements. It is

(a)E-mail: yhj@postech.ac.kr

shown that while the magnetically induced polarization variation in $\alpha$-$Cu_2V_2O_7$ can be accounted for neither by the spin current model nor the exchange striction mechanism, it is the $p$-$d$ hybridization between the transition metal Cu and ligand O via SOC that is essential for the account of its magnetoelectric effect.

**Experimentals.** – Polycrystalline samples of $\alpha$-$Cu_2V_2O_7$ were synthesized by a standard solid-state reaction method. Single crystals, on the other hand, were grown by a flux method using a mixture of $SrCO_3$ and $V_2O_5$ as a flux [15]. The obtained crystals were characterized by both powder and single-crystal X-ray diffraction (XRD; Rigaku, RINT2000). Neutron powder diffraction (NPD) experiments on powder samples were performed on the neutron powder diffractometer BT1 at NIST and possible magnetic structures were analyzed by carrying out the symmetry analysis using the program *SARAh*, and the refinement of magnetic structure was done with the *Fullprof* program. Magnetic property measurements were carried out using a commercial Quantum Design physical property measurement system (PPMS). Pyro-electric current and magnetoelectric (ME) current were measured with an electrometer (Keithley, 6517) combined with PPMS.

**Crystal structure.** – The crystal structure of $\alpha$-$Cu_2V_2O_7$ was determined by NPD and XRD and is in agreement with the previous report [13]. The structure belongs to the orthorhombic system with space group $Fdd2$ (no. 43), and its schematic diagram is shown in fig. 1(a). It consists of cross-linking chains of $[CuO_5]$ polyhedra with one chain parallel to the [011] direction and another parallel to $[0\bar{1}1]$ direction. These magnetic copper oxide chains are then separated by nonmagnetic $(V_2O_7)^{-4}$ anion groups. The local structure of the $[CuO_5]$ polyhedron is of central importance for the ME properties, and the schematic diagram is shown in fig. 1(b). The bond lengths were determined by XRD and NPD at 5 K; each Cu ion is surrounded by five oxygen ions, and four of them have shorter bonds of 1.91–1.94 Å to Cu and the apical oxygen has a longer bond of 2.56 Å. The $a$, $b$, and $c$ lattice parameters are 20.69 Å, 8.43 Å, and 6.44 Å, respectively [16]. As far as the point group $mm2$ of the system is concerned, the unit cell contains four inequivalent Cu sites due to different $[CuO_5]$ polyhedron orientations designated as Cu1, Cu2, Cu3, and Cu4 in fig. 1(c). Note that $mm2$ lacks inversion symmetry and thus $\alpha$-$Cu_2V_2O_7$ could be ferroelectric or pyroelectric. In the low-temperature phase with magnetic ordering, the Cu ions ($d^9$, $S = 1/2$) themselves become inequivalent due to the spin directions.

**Magnetic properties.** – Figure 2(a) is the plot of the susceptibility $\chi \equiv M/H$ (magnetization per unit field strength) of the single crystalline $\alpha$-$Cu_2V_2O_7$ in the $a$-direction as a function of temperature $T$. A measuring field $\mu_0H$ of 1 T was used to ensure sensitivity. For a field parallel to the [100] direction, $\chi$ exhibits a clear cusp
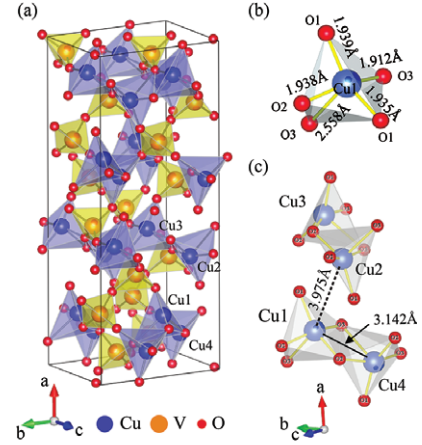


Fig. 1: (Color online) (a) Crystal structure of $\alpha$-$Cu_2V_2O_7$ with the Cu and V polyhedron colored in blue and yellow, respectively. Crystallographic axes are also shown. The lattice parameters are $a = 20.69$ Å, $b = 8.43$ Å, and $c = 6.44$ Å. (b) Local environment surrounding the Cu ion. Cu-O bond lengths, taken from neutron diffraction at 5 K, are indicated. (c) Four Cu sites with different $[CuO_5]$ orientations in the unit cell are shown. Edge sharing nearest neighbor Cu-Cu (3.142 Å) is indicated by a solid line, while the inter-chain neighbor Cu-Cu (3.975 Å) is indicated by a dotted line.
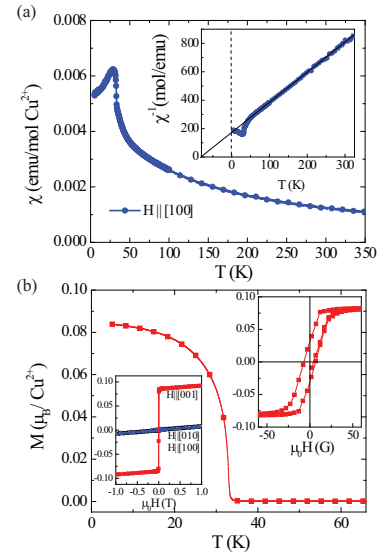


Fig. 2: (Color online) (a) Susceptibility $\chi$ of $\alpha$-$Cu_2V_2O_7$ measured with $\mu_0H = 1$ T along the $a$-direction is shown as a function of $T$. The inset displays $\chi^{-1}$ as a function of $T$; the line represents the Curie-Weiss law from which the Curie constant and the asymptotic Curie temperature are obtained. (b) The magnetization $M$ in the $c$-direction measured with a small field 50 G clearly identifies a ferromagnetic transition. The lower inset displays $M$-$H$ curves measured at $T = 10$ K. The upper inset is a magnified view of the low-field region of the $M$-$H$ curve.

at $T_N = 33.3$ K indicating an antiferromagnetic transition. Below $T_N$, however, $\chi$ does not decrease to zero as $T$ approaches zero. This fact may indicate that the system may not be a simple antiferromagnet. To check the

possibility, $M$ along the $c$-direction was measured with a small measuring field of 50 G. When a field is applied in the $c$-direction, the situation becomes strikingly different and spontaneous magnetization is detected below $T_N$. Figure 2(b) shows $M(T)$, expressed as the Bohr magneton $\mu_B$ per Cu ion, of $\alpha$-Cu$_2$V$_2$O$_7$ in the temperature range from 4 to 70 K. The $M$ measurements clearly identifies a ferromagnetic transition. In fact, Ponomarenko *et al.* studied polycrystalline samples and suggested that the spontaneous magnetization arose due to the ferrimagnetic or canted antiferromagnetic state because the saturated moment value 0.04 $\mu_B$ they obtained was very small [17,18]. For our single-crystal samples, the $M$-$H$ curve measured at $T = 10$ K shows that the moment value reaches 0.08 $\mu_B$ quickly at a small field and then increases slowly to 0.09 $\mu_B$ at 1 T for $H \parallel [001]$, as displayed in the lower inset of fig. 2(b). The magnified view of the $M$-$H$ curve in the low-field region, given in the upper inset, clearly illustrates weak ferromagnetism with a hysteresis behavior with remanent magnetization $M_r \approx 0.03 \mu_B$ and coercivity $\mu_0 H_c \approx 7$ G. Obviously, the hysteric behavior consists of two regimes, domain wall motion at low fields ($< 10$ G) and field-induced canting at higher fields.

In order to estimate the size of the intrinsic magnetic moment per Cu ion, we can utilize the susceptibility data in the paramagnetic region, that is, $\chi$ as a function of $T$ is analyzed in terms of the Curie-Weiss law,

$$\chi = \frac{C}{T - \Theta} \tag{1}$$

where $C$ is the Curie constant and $\Theta$ is the asymptotic Curie (or Curie-Weiss) temperature. Here *asymptotic* refers to the fact that the Curie-Weiss law holds well in the deep paramagnetic region. The effective magnetic moment $\mu_{\text{eff}}$ can be determined from the Curie constant. $\chi^{-1}$ as a function of $T$ is shown in the inset of fig. 2(a) and $\Theta$ and $\mu_{\text{eff}}$ were extracted by fitting the data to the Curie-Weiss law. The fit yielded $\Theta = -81.5$ K and $\mu_{\text{eff}} = 1.95 \mu_B$. Note that $\mu_{\text{eff}} = 1.95 \mu_B$ is larger than the spin-only value of $\mu = g\sqrt{1/2(1 + 1/2)} = 1.73 \mu_B$ for $S = 1/2$ with the $g$ factor 2. These analysis results reveal the facts that $g$ deviates from 2 in this system due to SOC and that the saturated magnetic moment of 0.09 $\mu_B$ is far smaller than the intrinsic value. The latter fact, in particular, supports the idea that spin canting occurring in the antiferromagnetic state is the origin of the small spontaneous magnetization. As a matter of fact, Pommer *et al.* already showed that the spin canting as well as the underlying antiferromagnetism in $\alpha$-Cu$_2$V$_2$O$_7$ can be accounted for in terms of the superexchange and DM interaction along the chain direction if the chain structure of edge-sharing CuO$_5$ polyhedra and the local distortion surrounding each Cu ion are taken into account [19]. Thus, it may be concluded from the magnetic measurements that in the ground state of $\alpha$-Cu$_2$V$_2$O$_7$, the Cu spins are ordered antiferromagnetically along the $a$-direction and canted magnetic moments occur along the $c$-direction.



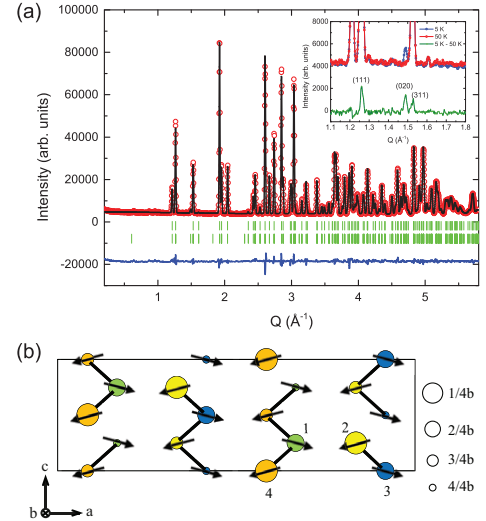Fig. 3: (Color online) (a) Neutron powder diffraction of $\alpha$-Cu$_2$V$_2$O$_7$ measured at 5 K. Circles are the experimental data and black lines represent the calculated intensities. Green bars represent nuclear and magnetic Bragg peak positions and blue lines indicate the difference between experimental data and calculation. The inset compares the data obtained at 5 K and 50 K. A magnetic peak appears at lower temperature. (b) Magnetic structure refined with $\Gamma_2$ representation, consisting of Cu$^{2+}$ spins antiferromagnetically aligned in the $a$-direction with small canting in the $c$-direction. Only copper ions are shown and the arrows denote spin directions. Four inequivalent Cu ions are colored in green (1), yellow (2), blue (3), and orange (4). The size of the circles represents the $b$-direction position and the solid lines connect nearest-neighbor Cu ions.

**Determination of the magnetic structure.** – The microscopic magnetic structure of $\alpha$-Cu$_2$V$_2$O$_7$ was investigated in detail by analyzing the NPD results [20]. The NPD data were collected at two temperatures below and above $T_N$, 5 K and 50 K. Figure 3(a) shows the NPD data measured at 5 K. The crystal structure refinement was performed with *Fullprof* and the optimal parameters obtained with space group $Fdd2$ are summarized in table 1. The inset of fig. 3(a) shows the NPD data at 5 K, 50 K and their difference. The characteristic wave vector for magnetic ordering was identified as $k_m = (0, 0, 0)$. An additional intensity at the (020) Bragg peak position which is forbidden by space group $Fdd2$, was observed at 5 K, indicating an antiferromagnetic arrangement of spins. Possible magnetic structures were inspected by carrying out a group theoretical analysis. The best-fit magnetic structure was obtained using basis vectors of $\Gamma_2$ irreducible representation [21]. The magnetic moment for each Cu ion in the unit cell is summarized in table 2. The ordered moment was 0.84 $\mu_B$ which is close to the expected spin moment of $S = 1/2$. Cu spins are ordered antiferromagnetically along the $a$-direction with a canting towards the $c$-direction. In this model, the finite magnetic moment along the $b$-axis, $M_b$, will produce an additional intensity at the (200) Bragg peak. The NPD data, however, do

Table 1: The crystal structural parameters of $\alpha$-Cu$_2$V$_2$O$_7$ with space group $Fdd2$ obtained at 5 K by refining the data shown in fig. 3 using the program *Fullprof*. $B_{\mathrm{iso}}$ is an isotropic thermal parameter expressed as $\exp(-B_{\mathrm{iso}}\sin^2\theta/\lambda^2)$, where $\theta$ is the scattering angle and $\lambda$ is the wavelength of the neutron. The lattice parameters are also shown.

| Atom $(W)$ | $x$ | $y$ | $z$ | $B_{\mathrm{iso}}$ ($\mathrm{\AA}^2$) |
|---|---|---|---|---|
| Cu $(16b)$ | 0.1658(1) | 0.3633(2) | 0.7500 | 0.24(3) |
| V $(16b)$ | 0.1964(10) | 0.4023(30) | 0.2602(46) | 0.30 |
| O1 $(16b)$ | 0.2457(1) | 0.5627(2) | 0.2704(3) | 0.48(3) |
| O2 $(16b)$ | 0.1446(1) | 0.4392(2) | 0.0260(4) | 0.39(4) |
| O3 $(16b)$ | 0.1619(1) | 0.3469(2) | 0.4540(3) | 0.39(4) |
| O4 $(8a)$ | 0.2500 | 0.2500 | 0.1509(4) | 0.67(6) |

$a = 20.6892(2)$ Å, $b = 8.4277(1)$ Å, $c = 6.43975(5)$ Å

Table 2: Magnetic moments for four inequivalent Cu ions obtained by refining the NPD data at 5 K with antiferromagnetic arrangements of spins with canting along the $c$-direction.

| Ion | $M_a$ | $M_b$ | $M_c$ | $\langle M \rangle$ |
|---|---|---|---|---|
| Cu1 | 0.797(35) | 0 | $-0.26(14)$ | 0.84(6) |
| Cu2 | $-0.797(35)$ | 0 | $-0.26(14)$ | 0.84(6) |
| Cu3 | 0.797(35) | 0 | $-0.26(14)$ | 0.84(6) |
| Cu4 | $-0.797(35)$ | 0 | $-0.26(14)$ | 0.84(6) |

not show any increase in the intensity at the (200) Bragg peak when cooled down below $T_N$. Therefore, $M_b$ was assumed to be zero in the refinement, and indeed it is also supported by the macroscopic magnetic measurements. A schematic diagram of the magnetic structure drawn from the neutron scattering results is presented in fig. 3(b).

**Magnetoelectric effect.** – We now turn to the ME effect of $\alpha$-Cu$_2$V$_2$O$_7$. Let us begin with the definition of ME tensors. We use $x$, $y$, and $z$ to denote the laboratory axes as opposed to the crystallographic axes $a$, $b$, and $c$. The ME tensors are defined by

$$P_i = \sum_{j=1}^{3} \alpha_{ij} H_j + \sum_{k,l=1}^{3} \beta_{ikl} H_k H_l + \ldots, \qquad (2)$$

where indices 1, 2, and 3 denote $x$, $y$, and $z$ axes, respectively. The laboratory axes coincide with the crystallographic ones in the present case, and thus these two sets are interchangeable. As noted in the previous section, if we consider atomic positions only, the crystal structure of $\alpha$-Cu$_2$V$_2$O$_7$ has $mm2$ point group symmetry. In the magnetically ordered phase below $T_N$, however, the magnetic order of the system change the symmetry from $mm2$ to $m'm'2$, where $m'$ denotes the antisymmetry of mirror reflection followed by time reversal operation. Under
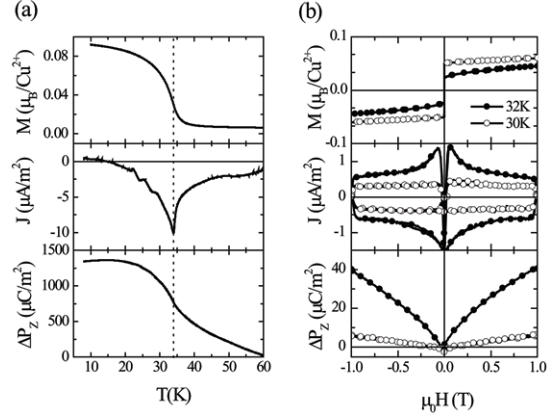


Fig. 4: (a) Magnetization $M$, pyroelectric current density $J$, and polarization $\Delta P_z$ (integrated current density) are shown as a function of temperature. Note that $J$ was measured with $\mu_0 H = 0$, while a small field of 50 G was used for $M$ measurements. (b) The same quantities are measured as a function of the magnetic field at fixed temperatures below $T_N$.

$m'm'2$, the diagonal elements are nonzero and all the off-diagonal elements are zero in the linear ME tensor, contrary to the case of $mm2$ where only the two off-diagonal elements $\alpha_{12}$ and $\alpha_{21}$ are nonzero. Nonzero components of the third-order ME tensor are $\beta_{113}$, $\beta_{223}$, $\beta_{322}$, $\beta_{311}$, and $\beta_{333}$ for both $mm2$ and $m'm'2$. Consequently, the induced polarization $P_z$ in the ordered phase with a field applied along the $c$-direction is given by

$$P_z(T < T_N) = \alpha_{33} H_z + \beta_{333} H_z^2. \qquad (3)$$

To identify the ME effect of $\alpha$-Cu$_2$V$_2$O$_7$, we first measured the electric polarization variation along the $c$-axis $\Delta P_z$ by measuring and integrating the pyrocurrent as a function of $T$ with $H = 0$. We then studied the ME effect by measuring the induced polarization $\Delta P_z$ as a function of $H \parallel c$ at fixed $T$. For pyroelectric measurements, a poling electric field was applied to a sample well above $T_N$, and the sample was cooled to 5 K and the current was measured on heating. In fig. 4(a) the magnetization $M$, the pyroelectric current density $J$, and $\Delta P_z$ are presented together as a function of $T$. The pyroelectric current density $J$ was measured without field, while the measuring field for $M$ was 50 G. Note that a sharp negative peak at $T_N$ is observed on heating in $J(T)$, and thus the polarization decreases rapidly in the vicinity of $T_N$. In integrating $J$ to obtain the polarization $\Delta P_z$, the zero point was chosen arbitrarily at $T > T_N$. It should be emphasized that the polarization remains nonzero even above $T_N$. We have also confirmed that the polarization is not switchable by electric poling up to the field strength of $E \approx 10\,\mathrm{kV/cm}$. This fact indicates that the $\alpha$-Cu$_2$V$_2$O$_7$ is pyroelectric rather than ferroelectric both above and below $T_N$.

If a magnetic field is applied to the system below $T_N$, additional polarization due to the ME effect is observed. In fig. 4(b), the magnetic-field dependence of $M$, $J$, and

$\Delta P_z$ at fixed temperatures is shown. In converting the current data $J(H)$ to the polarization change $\Delta P_z$, the $H = 0$ point was chosen as the reference point. Note that there is a very rapid change in the current density $J$ in the immediate vicinity of zero field associated with the low-field $M$ jump due to domain wall motion. This change was too fast to follow exactly in the present experimental setup. The variation of $\Delta P_z$ over the field variation to 1 T seen in fig. 4(b) is the magnetic-field–induced polarization accompanying the concurrent spin canting. It is of value to note that the polarization change $\Delta P_z$ shows a distinct nonlinear dependence on $H$ and also that $\Delta P_z$ is an even function of $H$. These facts, of course, indicate the importance of $\beta_{333}$. From fitting of the data at 33 K, $\alpha_{33}$ and $\beta_{333}$ are estimated to be $42.1 \pm 0.1$ ps/m and $-5.9 \pm 0.1$ as/A, respectively. To fully account for the evenness of the ME response in the presence of nonzero $\alpha_{33}$, one must take into account the domain effects [21].

**Possible microscopic model for polarization induced by spin canting.** – According to the neutron diffraction results for crystal and magnetic structures of $\alpha$-Cu$_2$V$_2$O$_7$, the spin structure of the system is neither of spiral type nor of collinear striction type. Since the $p$-$d$ hybridization mechanism does not impose particular restrictions on the magnetic order to generate ME effects, we attempt to account for the ME effect in $\alpha$-Cu$_2$V$_2$O$_7$ via this model. We first identify the local electric polarization by focusing on the local structure surrounding a Cu ion. For a single CuO$_5$ polyhedra with the Cu spin $\boldsymbol{S}$, the local electric dipole moment within the $p$-$d$ hybridization model is given by $\boldsymbol{P}^\alpha \propto \sum_{i=1}^{5}(\boldsymbol{S}^\alpha \cdot \boldsymbol{e}^{\alpha i})^2 \boldsymbol{e}^{\alpha i}$. Superscripts $\alpha$ and $i$ designate Cu and O ions, respectively, and $\boldsymbol{e}^{\alpha i}$ is the unit vector along the bond direction between the Cu ion and O ion. Since there exist four inequivalent CuO$_5$ polyhedrons in the unit cell, the polarization $\boldsymbol{P}$ is expressed as a sum over Cu ions:

$$\boldsymbol{P} \propto \sum_{\alpha=1}^{4}\sum_{i=1}^{5}(\boldsymbol{S}^\alpha \cdot \boldsymbol{e}^{\alpha i})^2 \boldsymbol{e}^{\alpha i}. \tag{4}$$

In $\alpha$-Cu$_2$V$_2$O$_7$, unlike the staggered antiferromagnetism seen in Ba$_2$CoGe$_2$O$_7$, the $M$ variation with magnetic field is dominated by spin canting along the $c$-axis for fields greater than $\sim 10$ G. Within the $p$-$d$ hybridization model where polarization is proportional to the square of the local spin moment, the magnetic-field–induced polarization would show both linear ($\alpha_{33}$) and nonlinear ($\beta_{333}$) dependence on $H$. To account for the ME effect quantitatively, we include the domain effects and assume that each spin in four Cu-O polyhedrons has the same canting angle $\theta$ in a given domain when $H \parallel c$ as illustrated in fig. 5(a) [21]. In fig. 5(b), we plot the polarization $P_z^{pd}$ as a function of $\theta$ by substituting Cu-O bonding direction and spin direction into eq. (4). It is noted that the local polarization variations along the $a$-axis due to Cu1(Cu3) and Cu2(Cu4) are the same but opposite in direction to make $P_x^{pd} = 0$. The situation is the same in the $b$-direction and thus $P_y^{pd} = 0$.
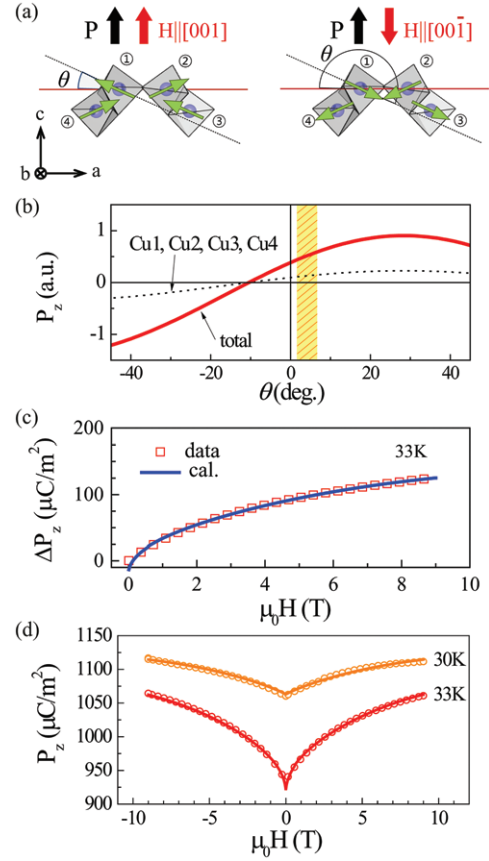


Fig. 5: (Color online) (a) Illustration of the spin structure with magnetic field along [001] and [00$\bar{1}$]. The number in the circle corresponds to each CuO$_5$ polyhedra site (Cu1 to Cu4). (b) Calculated polarization at each Cu site with respect to the spin canting angle within the $p$-$d$ hybridization model. We assume here that the canting angle of all spins is the same, that is, $\theta$ for Cu1 and Cu3, $\pi - \theta$ for Cu2 and Cu4 with $H \parallel c$-axis. (c) $\Delta P_z$ calculated polarization due to $p$-$d$ hybridization is shown along with experimental data at $T = 33$ K. (d) Polarization $P_z$ as a function of $\mu_0 H$ at 30 K and 33 K. The offset values at $H = 0$ are taken from the pyroelectric measurements shown in fig 4. Open circles and solid lines denote the experimental data and the calculation results, respectively.

Only the $c$-component of the polarization is nonzero because in this case all local contributions are identical in sign and magnitude. The total calculated polarization, as a function of $\theta$, is shown in fig. 5(b), and this variation can be expressed as $P_z^{pd}(\theta) = A\sin(2\theta + \eta) + C$ with $A = 1.15$, $C = -0.25$, and $\eta = 33°$. This result is consistent with the symmetry analysis: applying a field $H \parallel c$ does not change the $m'm'2$ symmetry and the three diagonal components of the linear ME tensor are expected to be nonzero. Let us consider $P_z^{pd}$ as a function of the magnetic field. Since $M$ is already known as a function of $H$, it is sufficient to express the canting angle as a function of $M$, that is, $\theta = \sin^{-1}(M/M_s)$ where saturation $M_s = 1\,\mu_B/\text{Cu}^{2+}$. For a given $M$ then, polarization becomes $P_z^{pd} \propto \sin(2\sin^{-1}(M/M_s) + \eta)$. (Constant $C$ can be absorbed into $\eta$.) Introducing canting angles $\theta_1(= \theta)$

and $\theta_2$ for the two domains separately and putting their ratio $\theta_1/\theta_2 = 1/\alpha$, we can write $M = (M_1 + M_2)/2 = (\sin(\theta) + \sin(\alpha\theta))/2$. For small $\theta$, $M \approx (1+\alpha)\theta/2$ and the polarization change is expressed as

$$\Delta P(M(H)) = A \left[ \sin \left( \frac{M}{M_s} \frac{4}{(\alpha+1)} + \eta \right) + \sin \left( \frac{M}{M_s} \frac{4\alpha}{(\alpha+1)} + \eta \right) \right] + B. \quad (5)$$

If the experimental data at $T = 33\,\mathrm{K}$ are fitted with eq. (5), $\alpha = 0.6$ gives an excellent fit as shown in fig. 5(c). The calculation (blue solid line) matches the experimental data (red open square) extremely well and the coefficients $A$ and $B$ are estimated to be $3190 \pm 5\,\mu\mathrm{C/m^2}$ and $-3550 \pm 5\,\mu\mathrm{C/m^2}$, respectively. The canting angle changes from $2\,^\circ$ to $7\,^\circ$ when an applied field changes from 0 to 9 T, corresponding to the hatched region in fig. 5(b). Figure 5(d) displays the full range of data and calculation results at 30 K and 33 K.

**Conclusions.** – We studied the structural, magnetic, and magnetoelectric properties of $\alpha$-$\mathrm{Cu_2V_2O_7}$ in both monocrystalline and polycrystalline forms. The magnetic measurements revealed, in particular, the underlying magnetic structure of canted antiferromagnetism with easy $a$-axis and canting $c$-axis. When an external magnetic field is applied along the $c$-direction, additional magnetization is induced by further spin canting and the induced magnetization is accompanied by polarization. The $p$-$d$ hybridization model adequately accounts for the observed magnetoelectric effect. The present study in turn implies that the $p$-$d$ hybridization mechanism would be quite ubiquitous in oxide materials and polarization can be induced by spin canting in antiferromagnetic systems. It is noted that the polarization in the $p$-$d$ hybridization scheme is of electronic origin in contrast to the ion displacement type occurring in the spin current mechanism or exchange striction [22]. We may keep in mind, in the search for new magnetoelectric materials, that while materials with particular magnetic structures are frequently sought after based on the spin current or exchange striction mechanisms, a reservoir of candidate materials with $p$-$d$ hybridization might be far greater.

$$* * *$$

REFERENCES

[1] KIMURA T., GOTO T., SHINTANI H., ISHIZAKA K., ARIMA T. and TOKURA Y., *Nature*, **426** (2003) 55.

[2] HUR N., PARK S., SHARMA P. A., AHN J. S., GUHA S. and CHEONG S.-W., *Nature*, **429** (2004) 392.

[3] EERENSTEIN W., MATHUR N. D. and SCOTT F., *Nature*, **442** (2006) 759.

[4] KATSURA H., NAGAOSA N. and BALATSKY A. V., *Phys. Rev. Lett.*, **95** (2005) 057205.

[5] SERGIENKO I. A. and DAGOTTO E., *Phys. Rev. B*, **73** (2006) 9094434.

[6] ARIMA T., TOKUNAGA A., GOTO T., KIMURA H., NODA Y. and TOKURA Y., *Phys. Rev. Lett.*, **96** (2006) 097202.

[7] CHOI Y. J., YI H. T., LEE S., HUANG Q., KIRYUKHIN V. and CHEONG S.-W., *Phys. Rev. Lett.*, **100** (2008) 047601.

[8] ARIMA T.-H., *J. Phys. Soc. Jpn.*, **76** (2007) 073702.

[9] JIA C., ONODA S., NAGAOSA N. and HAN J. H., *Phys. Rev. B*, **76** (2007) 144424.

[10] YI H., CHOI Y. J., LEE S. and CHEONG S.-W., *Appl. Phys. Lett.*, **92** (2008) 212904.

[11] MURAKAWA H., ONOSE Y., MIYAHARA S., FURUKAWA N. and TOKURA Y., *Phys. Rev. Lett.*, **105** (2010) 137202.

[12] KHANH N. D., ABE N., KUBO K., AKAKI M., TOKUNAGA M., SASAKI T. and ARIMA T., *Phys. Rev. B*, **87** (2013) 184416.

[13] SÁNCHEZ-ANDÚJAR M., YÁÑEZ-VILAR S., MIRA J., BISKUP N., RIVAS J., CASTRO-GARCIA S. and SEÑARIS-RODRIGUEZ M. A., *J. Appl. Phys.*, **109** (2011) 054106.

[14] SANNIGRAHI J., BHOWAL S., GIRI S., MAJUMDAR S. and DASGUPTA I., *Phys. Rev. B*, **91** (2015) 220407(R).

[15] HE ZHANGZHEN and UEDA YUTAKA, *Phys. Rev. B*, **77** (2008) 052402.

[16] MERCURIO-LAVAUD D. and FRIT B., *Acta Crystallogr., Sect. B*, **29** (1973) 2737.

[17] PONOMARENKO L. A., VASIL'EV A. N., ANTIPOV E. V. and VELIKODNY YU. A., *Physica B: Condens. Matter*, **284-288**, Part 2 (2000) 1459.

[18] TOUAIHER M., RISSOULI K., BENKHOUJA K., TAIBI M., ARIDE J., BOUKHARI A. and HEULIN B., *Mater. Chem. Phys.*, **85** (2004) 41.

[19] POMMER J., KATAEV V., CHOI K.-Y., LEMMENS P., IONESCU A., PASHKEVICH YU., FREIMUTH A. and GÜNTHERODT G., *Phys. Rev. B*, **67** (2003) 214410.

[20] GITGEATPONG G., ZHAO Y., AVDEEV M., PILTZ R. O., SATA T. J. and MATAN K., *Phys. Rev. B*, **92** (2015) 024423.

[21] See the supplementary material at `https://goo.gl/DohxOI`.

[22] YANG I. K., KIM J., LEE S. H., CHEONG S.-W. and JEONG Y. H., *Appl. Phys. Lett.*, **106** (2015) 152902.